Journal of Breast Cancer

J Breast Cancer 2012 March; 15(1): 57-64 http://dx.doi.org/10.4048/jbc.2012.15.1.57

ORIGINAL ARTICLE

Imaging Findings of Invasive Micropapillary Carcinoma of the Breast

Se Un Yun, Bo Bae Choi, Kwang Sun Shu[1], Seong Min Kim[2], Young Duk Seo[2], Jin Sun Lee[3], Eil Sung Chang[3]

Departments of Radiology, [1]Pathology, [2]Nuclear Medicine, and [3]Surgery, Chungnam National University Hospital, Daejeon, Korea

Purpose: The purpose of this study is to evaluate imaging and histopathologic findings including the immunohistochemical characteristics of invasive micropapillary carcinoma (IMPC) of the breast. **Methods:** Twenty-nine patients diagnosed with IMPC were included in the present study. Mammographic, sonographic, and magnetic resonance imaging (MRI) findings were analyzed retrospectively according to the American College of Radiology Breast Imaging Reporting and Data System lexicon. ^{18}F-fluorodeoxyglucose positron emission tomography-computed tomography (PET-CT) findings were also evaluated. Microscopic slides of surgical specimens were reviewed in consensus by two pathologists with a specialty in breast pathology. **Results:** Most IMPCs presented as a high density irregular mass with a non-circumscribed margin associated with microcalcifications on mammography, as an irregular hypoechoic mass with a spiculated margin on ultrasound, and as irregular spiculated masses with washout patterns on MRI. PET-CT showed a high maximum standardized uptake value (SUVmax) (mean, 11.2). Axillary nodal metastases were identified in 65.5% of the patients. Immunohistochemical studies showed high positivities for estrogen receptor and c-erbB-2 (93.1% and 51.7%, respectively). **Conclusion:** Even though the imaging characteristics of IMPCs are not distinguishable from typical invasive ductal carcinomas, this tumor type frequently results in nodal metastases and high positivities for both estrogen receptor and c-erbB-2. The high SUVmax value that is apparent on PET-CT might be helpful in the diagnosis of IMPC.

Key Words: *Breast, Carcinoma, Magnetic resonance imaging, Mammography, Ultrasound*

INTRODUCTION

Invasive micropapillary carcinoma (IMPC) is a rare, clinically aggressive variant of invasive ductal carcinoma that accounts for 0.7-3% of all breast cancer cases. It is associated with a high incidence of axillary lymph node metastases, frequent local recurrence, and a poor clinical outcome. A diagnosis of IMPC was first described in the pathology literature by Petersen [1] in 1993, and it was newly listed in the World Health Organization (WHO) classification of breast cancer in 2003. This carcinoma is characterized histopathologically by tubuloalveolar or pseudopapillary structures lacking a fibrovascular core and surrounded by clear, empty spaces [2-4]. While many studies have been carried out of IMPC that focus on pathologic findings [3,5], to our knowledge, only a few studies focus on the radiologic findings of IMPC [2,5,6]. Therefore, we retrospectively evaluated imaging and histopathologic findings including the immunohistochemical characteristics of IMPC.

Correspondence: **Bo Bae Choi**
Department of Radiology, Chungnam National University Hospital, 33 Munhwa-ro, Jung-gu, Daejeon 301-721, Korea
Tel: +82-42-280-8571, Fax: +82-42-253-0061
E-mail: med20@hanmail.net

Received: May 26, 2011 **Accepted:** November 7, 2011

METHODS

Seventy-three patients diagnosed with IMPCs from November 2001 to November 2010 were identified on the basis of a search of the pathologic database. On the basis of the surgical specimen, we excluded 9 patients diagnosed with invasive ductal carcinoma (IDC) (n = 8) and mucinous carcinoma (n = 1), despite being diagnosed with IMPC on the basis of core or excisional biopsies. We excluded 6 patients who underwent core needle biopsy only without surgery. IMPC in this study included cases with a more than 90% IMPC component. Therefore, we also excluded 26 cases that contained non-micropapillary components, such as IDC (n = 18), invasive cribriform carcinoma (n = 4), mucinous carcinoma (n = 2), tubular carcinoma (n = 1), and microinvasive ductal carcinoma (n = 1). Three further patients were excluded because radiologic images were not available for review. In total, 29 patients were enrolled in this study.

For mammograms, craniocaudal and mediolateral oblique

http://ejbc.kr | pISSN 1738-6756 eISSN 2092-9900

views were obtained using Mammomat 3000 (Siemens Medical Solutions, Solna, Sweden) and Lorad M3 (Hologic Inc., Boston, USA) mammography units. All mammograms and ultrasonograms were retrospectively reviewed in consensus by one radiologist with 5 years of experience in breast imaging and by one resident. Parenchymal patterns on mammograms were categorized as either one of the following: pattern 1, almost entirely fatty; pattern 2, scattered fibroglandular tissue; pattern 3, heterogeneously dense; or pattern 4, extremely dense. Each mammographic lesion was analyzed according to mass characteristics (i.e., shape, margin, and density), presence of architectural distortion, and type of microcalcification (according to the American College of Radiology [ACR] breast imaging reporting and data system [ACR BI-RADS] lexicon).

Ultrasound (US) was performed using a HDI 5000 (Advanced Technology Laboratories, Bothell, USA) or iU22 (Philips Ultrasound, Bothell, USA) US systems with a 5-12 MHz linear probe. We examined both breasts and the axillary lymph nodes. US images were reviewed for shape, orientation, margin, boundary, echogenicity, posterior acoustic features, and associated calcifications, and were categorized according to the ACR BI-RADS final assessment. The largest diameter obtained from either sagittal or transverse views was recorded as the maximum tumor diameter. On the basis of previous studies, we defined a metastatic axillary lymph node on US when the lymph node had at least one of the following findings: a mean longitudinal-transverse axis ratio of less than 1.5; the presence of eccentric cortical thickening; or the loss of a central fatty hilum [7].

Magnetic resonance imaging (MRI) was performed using a 1.5-T scanner (Signa Excite; GE Healthcare System, Milwaukee, USA) equipped with a breast coil. Images were acquired in axial plane with the following sequences: axial, T2-weighted, fat-suppressed, fast spin-echo imaging (TR/TE = 5,000/86, a flip angle of 90°, a field of view [FOV] of 300 mm, an acquisition matrix of 256 × 256, the number of excitations [NEX] of 3, and a 4.5-mm slice thickness); pre- and post-contrast, axial, and T1-weighted 3D fast spoiled gradient-recalled echo sequence with parallel volume imaging (VIBRANT; GE Healthcare System) (TR/TE = 6.5/3.1, a flip angle of 10°, a FOV of 300 mm, an acquisition matrix of 350 × 350, a NEX of 1, and a 1.1-mm slice thickness). To provide image contrast, Gadodiamide (Omniscan; GE Healthcare AS, Oslo, Norway) was administered with an intravenous bolus injection (0.2 mmol per kg of body weight) at 3 mL/sec. Imaging was performed before the patients were given the intravenous bolus injection of the contrast material and four times over a period of 7.3 minutes after the patients were given the injection. Image post-processing, using the first contrast-enhanced series, included subtraction of unenhanced images from enhanced images, sagittal reformations, and 3D maximum-intensity projections. Interpretation of the degree and patterns of enhancement was performed by visual assessment. The feature of abnormal enhancement was classified according to the ACR BI-RADS MRI lexicon. Associated findings, such as nipple retraction, skin thickening, lymphadenopathy, hematoma, and invasion of the pectoralis muscle and chest wall, were recorded.

^{18}F-Fluorogeoxyglucose (FDG) PET-computed tomography (CT) imaging was performed using a Discovery ST-16 system (GE Medical Systems). After fasting for at least 6 hours, normal fasting blood glucose levels were determined to be < 150 mg/dL for all patients. Patients ingested more than 500 mL of fluid for adequate urination. An intravenous injection of 8.14 MBq/kg (0.22 mCi/kg) of FDG was then given, and the subject rested for approximately 1 hour. Pre-contrast CT scanning was performed using 16-channel CT from the skull base to the upper thigh prior to PET. PET was then immediately conducted over the same body region using 5-7 bed positions with a 3-minute acquisition time per bed position. CT data were used for attenuation correction and anatomical correlation with the PET data. Data were evaluated on a workstation (Advanced Workstation, version 4.3; GE Medical Systems) by a nuclear medicine physician and a resident. PET scans were analyzed visually and semi-quantitatively. FDG uptake was considered to be abnormal on visual analysis when the uptake in the region of the primary tumor was substantially higher than the background uptake in the contralateral breast or axilla. The highest recorded FDG uptake was semi-quantitatively analyzed after being corrected for radioactive decay, according to the following formula: maximum standardized uptake value (SUVmax) = mean region of interest activity (mCi/mL)/injected dose (mCi)/body weight (g).

Microscopic slides of surgical specimens were reviewed in consensus by two pathologists with a specialty in breast pathology. The presence of lymphovascular invasion and lymph node metastasis was evaluated, as well as the immunohistochemical characteristics. Immunohistochemical analyses for estrogen receptor (ER), progesterone receptor (PR), and c-erbB-2 were performed. Four sections were cut from the tissue microarray blocks and placed on coated slides. The slides were baked in an oven overnight at 55°C to enhance adhesion of the sections to the slides. Deparaffinization in xylene and graded alcohol followed. Prediluted antibodies against ER (1:240; Immunotech, Marseille, France), PR (1:240; Novocastra, Newcastle, UK), and c-erbB-2 (1:400; Dako, Glostrup, Denmark) were obtained from commercial sources. Immunolocalization was performed using an LSAB kit (Dako, Carpinteria, USA). All assays were carried out prospectively in an automated immunostainer (Dako, Carpinteria, USA). Antibody-antigen re-

http://dx.doi.org/10.4048/jbc.2012.15.1.57

activity was visualized using diaminobenzidine and counterstaining with Meyer's hematoxylin. The status of ER, PR, and c-erbB-2 were evaluated according to the American Society of Clinical Oncology/College of American Pathologists (ASCO/CAP) guidelines for immunohistochemistry. ER and PR are considered positive if there are at least 1% positive tumor nuclei. The immunohistochemical (IHC) staining for c-erbB-2 was scored as 0 (no staining), 1+ (weak, incomplete membrane staining in any proportion of tumor cells), 2+ (complete membrane staining that is either nonuniform or weak in intensity but with obvious circumferential distribution in at least 10% of cells), or 3+ (uniform intense membrane staining of > 30% of invasive tumor cells). And IHC staining results for c-erbB-2 were categorized as nega- tive (0 or 1+), equivocal (2+), or positive (3+). Equivocal cases were studied by fluorescent *in situ* hybridization (FISH) to determine c-erbB-2 gene amplification.

Two-color FISH was done on a 3 μm-thick consecutive microarray sections. Before hybridization, the sections were deparaffinized, air dried, and dehydrated in 100% ethanol after incubation at 56°C for 24 hours. Microarray slides were treated in wash buffer (Vysis Inc., Downers Grove, USA) for 3 minutes after treatment with 0.2 N HCl for 20 minutes. Pretreatment solution (Vysis Inc.) at 80°C was applied for 30 minutes and the slides were washed with purified water. Slides were treated with wash buffer twice for 5 minutes serially. Immersed slides in protease solution (Vysis Inc.) at 37°C was applied for 10 minutes and the slides were washed with wash buffer at 45-50°C and air dried. Slides were fixed in 10% buffered formalin for 10 minutes and then washed with wash buffer at 45-50°C. For denaturation, slides were immersed in denaturation solution (Vysis Inc.) for 5 minutes at 72°C followed by dehydration with 70%, 85%, and 100% ethanol serially at 45-50°C. For hybridization, 20 μL LSI HER-2/CEP17 probe (PathVision™; Vysis Inc.) was applied and a coverslip was applied over the probe. After overnight hybridization at 37°C in a humidified chamber, the slides were washed with 72°C post-hybridization wash buffer (PHWB; Vysis Inc.) for 2 minutes. Nuclei were counterstained with 20 μL 4,6-diamino-2-phenylindole (DAPI; Vysis Inc.). The centromere 17 (CEP) and HER2 copy numbers were counted in the predominant tumor cell population. Hybridization signals were enumerated by the ratio of orange signals for c-erbB-2 to green signals for CEP in morphologically intact and nonoverlapping nuclei. At least 2.2 times more c-erbB-2 signals than CEP17 signals in the tumor cells was considered as the criterion for c-erbB-2 amplification.

RESULTS

The mean age of the 29 patients in this study was 48.9 years (range, 27-73 years). Twenty-eight patients were women and 1 patient was a man. The mean size of breast cancer on US was 2.2 cm (range, 0.6-8.0 cm). The initial manifestation of cancer was a palpable mass in 19 patients (65.5%), a screening mammographic abnormality in 7 patients (24.1%), nipple discharge in 1 patient (3.4%), a palpable mass with nipple discharge in 1 patient (3.4%), and a regular, post-surgical follow-up for 1 patient (3.4%). The location of breast cancer was on the left breast in 15 patients (51.7%), and on the right in 14 patients (48.3%).

In total, 24 patients underwent mammography and the mammographic findings are presented in Table 1. Masses were noted in 13 patients (54.2%) (Figure 1A), asymmetry or focal asymmetry was noted in 5 patients (20.8%), microcalcifications only without mass or asymmetry were observed in 5 patients (20.8 %), and no abnormalities were found in 1 patient (4.2%). The most common findings for masses were an irregular shape (9 of 13; 69.2%), a non-circumscribed margin (11 of 13; 84.6%), and a high density (12 of 13; 92.3%). Microcalcifications were visible in 16 patients (66.7%). The shape of microcalcifications was fine pleomorphic in 9 patients (56.3%) (Figure 2A), fine

Table 1. Mammographic findings of invasive micropapillary carcinoma

Findings (n = 24)	No. (%)
Negative	1 (4.2)
Mass	13 (54.2)
(Focal) asymmetry	5 (20.8)
Calcification only	5 (20.8)
Shape (n = 13)	
Round	1 (7.7)
Oval	2 (15.4)
Lobular	1 (7.7)
Irregular	9 (69.2)
Margin (n = 13)	
Circumscribed	2 (15.4)
Microlobulated	2 (15.4)
Obscured	3 (23.1)
Indistinct	1 (7.7)
Spiculated	5 (38.5)
Density (n = 13)	
High density	12 (92.3)
Iso density	1 (7.7)
Shape of associated microcalcifications (n = 16)	
Round	2 (12.5)
Punctate	2 (12.5)
Amorphous	1 (6.3)
Fine pleomorphic	9 (56.3)
Fine linear or fine linear branching	2 (12.5)
Distribution of microcalcifications (n = 16)	
Regional	1 (6.3)
Clustered	6 (37.5)
Linear	1 (6.3)
Segmental	8 (50.0)

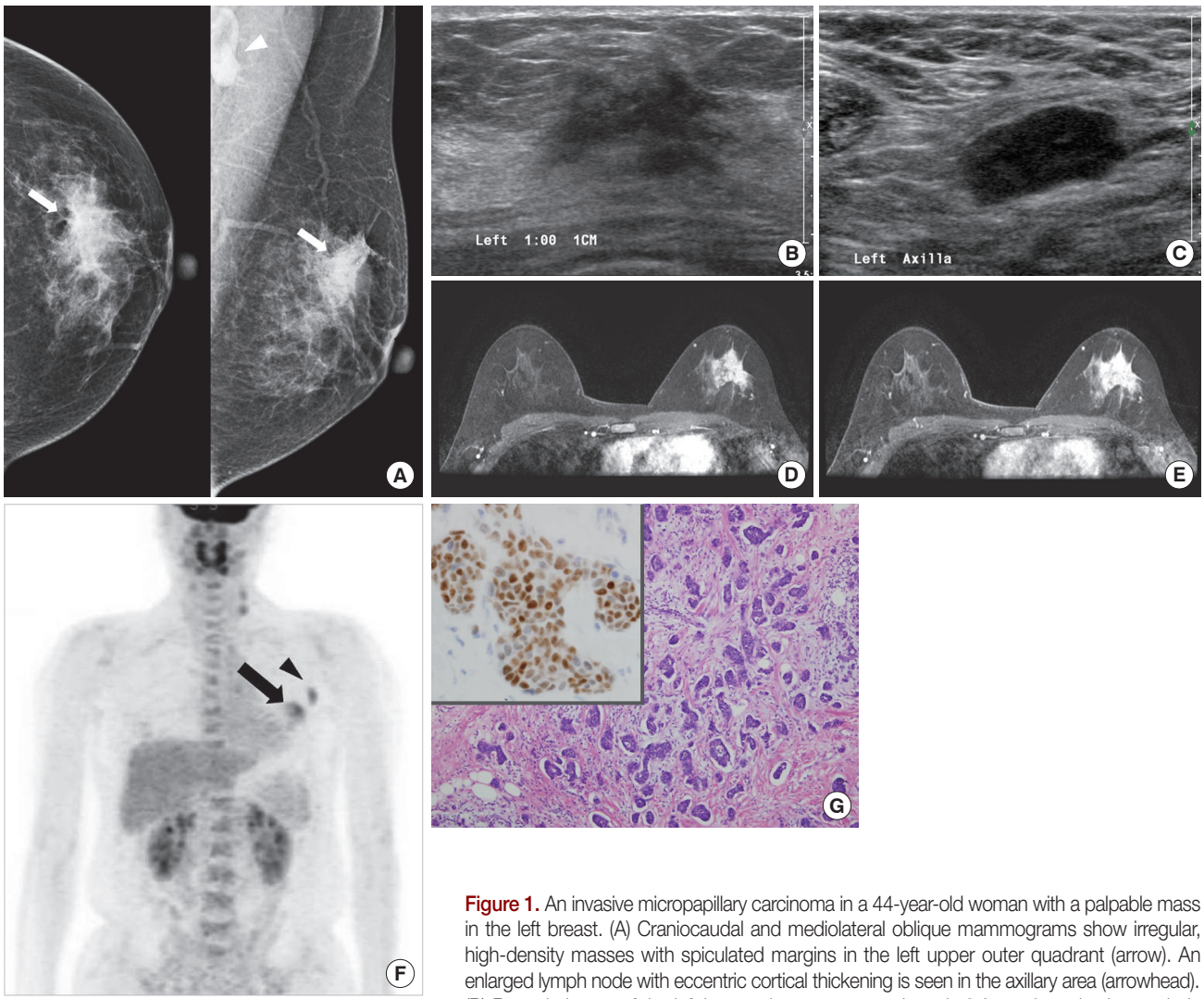

Figure 1. An invasive micropapillary carcinoma in a 44-year-old woman with a palpable mass in the left breast. (A) Craniocaudal and mediolateral oblique mammograms show irregular, high-density masses with spiculated margins in the left upper outer quadrant (arrow). An enlarged lymph node with eccentric cortical thickening is seen in the axillary area (arrowhead). (B) B-mode image of the left breast shows an approximately 2.6 cm, irregular, hypoechoic mass with spiculated margins in the 1 o'clock position. (C) B-mode image of the left axilla shows an approximately 2.2 cm, enlarged lymph node with cortical thickening and obliteration of the central fat hilum, which suggests a metastatic lymph node. The lymph node was pathologically confirmed as metastasis. (D, E) Axial, dynamic, contrast-enhanced, T1-weighted MR images of the left breast 2 minutes (D) and 6 minutes (E) after contrast injection show an approximately 3.3 cm, heterogeneous, enhanced mass in the upper outer quadrant. The kinetic pattern was evaluated visually and showed a persistent pattern. (F) ^{18}F-FDG PET maximum intensity projection image shows a subtle increased glucose metabolism (SUVmax=4.6) in the left breast (arrow). Increased glucose metabolism (SUVmax=4.0) is seen in the left axillary lymph node (arrowhead). (G) Photomicrography shows clusters of tumor cells in a micropapillary arrangement that appears to be within clear spaces (H&E stain, ×100; Inlet: positive immunohistochemical stain for estrogen receptor, ×400).

linear or fine linear branching in 2 patients (12.5%), round in 2 patients (12.5%), punctate in 2 patients (12.5%), and amorphous in 1 patient (6.3%). The distribution of microcalcifications was segmental in 8 patients (50.0%) (Figure 2A), clustered in 6 patients (37.5%), regional in 1 patient (6.3%), and linear in 1 patient (6.3%).

US was performed on 29 patients and the sonographic features of masses are presented in Table 2 (Figure 1B). The following characteristics of masses were most common: an irregular shape in 25 patients (86.2%), a parallel orientation in 25 patients (86.2%), a spiculated margin in 17 patients (58.6%), an abrupt interface in 22 patients (75.9%), and hypoechoic pattern in 27 patients (93.1%). The posterior acoustic feature was negative in 20 masses (69.0%) and posterior acoustic shadowing was present in 9 masses (31.0%). Associated findings were ductal dilatation in 3 patients (10.3%) and lymphedema in 1 patient (3.4%). On the basis of the ACR BI-RADS final assessment, 24 cases (82.8%) were classified as category 5 (i.e., highly suggestive of malignancy; Figures 1B, 2B); 4 cases (13.8%) as category 4 (i.e., suspicious abnormality); and 1 case (3.4%) as

http://dx.doi.org/10.4048/jbc.2012.15.1.57

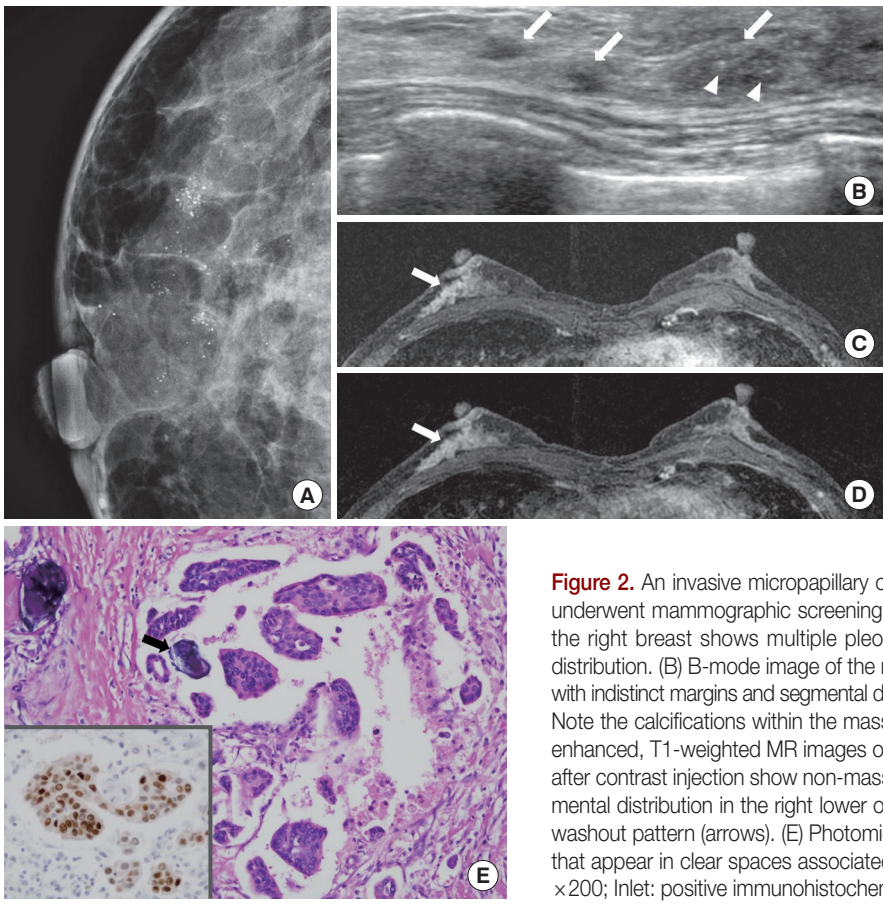

Figure 2. An invasive micropapillary carcinoma (IMPC) in a 60-year-old woman who underwent mammographic screening. (A) A magnified craniocaudal mammogram of the right breast shows multiple pleomorphic microcalcifications with a segmental distribution. (B) B-mode image of the right breast shows multiple hypoechoic masses with indistinct margins and segmental distributions in the twelve o'clock position (arrows). Note the calcifications within the mass (arrowheads). (C, D) Axial, dynamic, contrast-enhanced, T1-weighted MR images of the left breast 2 minutes (C) and 6 minutes (D) after contrast injection show non-mass-like, heterogeneous enhancement with a segmental distribution in the right lower outer quadrant. A kinetic curve analysis showed washout pattern (arrows). (E) Photomicrography shows tumor cells in glands or nests that appear in clear spaces associated with microcalcification foci (arrow) (H&E stain, ×200; Inlet: positive immunohistochemical stain for estrogen receptor, ×200).

Table 2. Sonographic findings of invasive micropapillary carcinoma

Findings (n=29)	No. (%)
Shape	
Oval	3 (10.3)
Round	1 (3.4)
Irregular	25 (86.2)
Orientation	
Parallel	25 (86.2)
Not parallel	4 (13.8)
Margin	
Circumscribed	3 (10.3)
Indistinct	1 (3.4)
Angular	5 (17.2)
Microlobulated	3 (10.3)
Spiculated	17 (58.6)
Lesion boundary	
Abrupt interface	22 (75.9)
Echogenic halo	7 (24.1)
Echo pattern	
Anechoic	1 (3.4)
Complex	1 (3.4)
Hypoechoic	27 (93.1)
Posterior acoustic features	
No posterior acoustic feature	20 (69.0)
Shadowing	9 (31.0)

category 3 (i.e., probably benign finding). We evaluated axillary lymph nodes in 29 cases and 13 patients (44.8%) were suspected to have metastatic lymph nodes (Figure 1C). All of these 13 patients were confirmed to have metastatic lymph nodes on pathological examination. Six patients with negative findings on the US of the axillary lymph node had metastatic lymph nodes on pathologic examination.

MRI was performed in 18 patients and findings are presented in Table 3. Enhanced masses were noted in 11 patients (61.1%) (Figure 1D, E), while non-mass-like enhancement was observed in 7 patients (38.9%) (Figure 2C). The most common mass features were an irregular shape (7 of 11; 63.6%), irregular margins (5 of 11; 45.5%), and heterogeneous internal enhancement (9 of 11; 81.8%) (Figure 1D, E). All 7 patients who presented with non-mass-like enhancement showed segmental distribution, and 6 of these 7 patients (85.7%) presented with heterogeneous internal enhancement (Figure 2C). We performed kinetic curve analysis on 15 patients. The most common pattern was a washout pattern in 6 patients (40.0%) (Figure 2C, D). Associated findings were nipple retraction in 1 patient (5.6%), hematoma in 1 patient (5.6%), and diffuse skin thickening in 1 patient (5.6%).

Table 3. Magnetic resonance imaging findings of invasive micropapillary carcinoma

Findings (n=18)	No. (%)
Mass	11
Shape	
Oval	2 (18.2)
Lobular	2 (18.2)
Irregular	7 (63.6)
Margin	
Smooth	2 (18.2)
Irregular	5 (45.5)
Spiculated	4 (36.4)
Non-mass	7
Kinetic curve assessment at delayed phase (n=15)	
Persistent	4 (26.7)
Plateau	5 (33.3)
Washout	6 (40.0)

^{18}F-FDG PET-CT was performed in 16 patients and all primary cancers showed FDG uptake (Figure 1F). The mean SUVmax value of primary breast cancers was 11.2 (range, 2.2-48.3). Axillary lymph nodes showed FDG uptake in 12 of 16 patients, and metastases were suspected in 12 patients (75.0%) (Figure 1F). All of these 12 patients were confirmed to have metastatic lymph nodes on pathological examination. Four patients with negative finding on ^{18}F-FDG PET-CT of axillary lymph node had metastatic lymph nodes on pathologic examination. In 2 patients, distant metastases to the liver, the lungs, bone, and intercostal muscles were seen.

Twenty-five patients underwent a modified radical mastectomy and 4 patients underwent a lumpectomy. Of the 29 surgical specimens, lymphovascular invasion was found in 27 (93.1%), and axillary nodal metastases were identified in 19 tumors (65.5%). The mean number of metastatic axillary lymph nodes was 6.6 (range, 1-23). Immunohistochemical analyses were available for 29 carcinomas. Study of primary breast cancer showed the expression of ERs in 93.1% of the cases (27 of 29) (Figures 1G, 2E) and PRs in 58.6% of the cases (17 of 29). For the c-erbB-2, a IHC score of 0 was shown in 8 cases (27.6%), 1+ in 4 cases (13.8%), 2+ in 5 cases (17.2%), and 3+ in 12 cases (41.4%). Three out of the 5 cases scored as 2+ showed gene amplification by FISH. Therefore, overexpression of the c-erbB-2 protein was observed in 51.7% of the cases (15 of 29).

Follow-up information was available for 27 patients. The mean follow-up period was 26.7 months (range, 1-68 months). Recurrence was noted in 4 patients: 2 in contralateral breast tissues and 2 in liver, lung, brain, and bone. Of these latter 2 patients, one died after 4 months while the other died after 32 months.

DISCUSSION

IMPC is an uncommon, clinically aggressive variant of IDC that accounts for 1.7-3% of all cases of breast cancer. In the 2003 WHO classification of breast tumors, IMPC was listed as a subtype of invasive carcinoma; however, no percentage of the IMPC component within the tumor was proposed as a criterion for diagnosis [8]. In the literature, no consensus opinion has been reached regarding the amount of IMPC required to make a diagnosis and determine the type of IMPC [3,9]. Regardless of the extent of the micropapillary component, tumors with any amount of this unique histologic pattern have a more aggressive clinical behavior and poorer prognosis with a high degree of lymph node involvement [2-4,9]. The most common clinical manifestation of IMPC is a palpable mass [2,5,6]. Similarly, we also found that palpable masses (19 of 29; 65.5%) were the most common clinical manifestation. Although only a few studies concerning IMPC imaging findings have been carried out, previous studies have reported that IMPCs may present as irregular, spiculated or indistinct, high-density masses on mammography, and as irregular, indistinct or microlobulated, hypoechoic masses on US [2,5,6]. In our study, masses were the most common finding on mammography (13 of 24; 54.2%), presenting as an irregular shape (9 of 13; 69.2%), a spiculated margin (5 of 13; 38.5%), and a high density (12 of 13; 92.3%) in most cases. Sonographic findings showed an irregular shape (25 of 29; 86.2%), a spiculated margin (17 of 29; 58.6%), a parallel orientation (25 of 29; 86.2%), hypoechoic pattern (27 of 29; 93.1%), and an abrupt interface boundary (22 of 29; 75.9%) as the most common features. Our results are in agreement with previous studies where microcalcifications were reported in 43-68% of the cases [2,5,6]. We found that microcalcifications presented in 66.7% (16 of 24) of the patients, which is similar to the result of a study conducted by Kim et al. [6] in which a 68% prevalence was observed, and by Adrada et al. [2] in which a 66% prevalence was noted. The shape of microcalcifications was indeterminate or highly suggestive of malignancy in most cases (12 of 16, 75.0%).

Only a few studies of MRI findings for IMPCs have been previously conducted [2,10]. In these studies, IMPCs presented as irregular, spiculated masses with early rapid initial enhancement and delayed washout or plateau pattern in dynamic contrast-enhanced studies [2,10]. We performed MRI in 18 patients, and the most common findings were irregular masses (7 of 18; 38.9%) with irregular or spiculated margins (9 of 18; 50.0%), and washout patterns (6 of 15; 40.0%) based on kinetic curve analysis. These results are similar to those reported in the previous studies.

To our knowledge, there are no other studies concerning

http://dx.doi.org/10.4048/jbc.2012.15.1.57

PET-CT findings of IMPCs. In our study, all 16 patients who were imaged with PET-CT showed FDG uptake in the primary breast cancer. Many previous studies have reported that there is a relationship between the SUV level and the following: histologic nuclear grade, incidence of lymph node metastasis, and hormonal receptor status [9-12]. Furthermore, a high uptake of ^{18}F-FDG is predictive of a poor prognosis in patients with primary breast cancer; the mean SUVmax value of primary tumors with axillary metastases is significantly higher (range, 4.1-7.4) than tumors with no axillary lymph node involvement or distant metastases (range, 2.8-5.2) [11-14]. In our study, the mean SUVmax value of the primary tumor was 11.2 (range, 2.2-48.3). A high SUVmax value may suggest a poor prognosis for IMPCs.

IMPCs have a high propensity for lymphatic and lymph nodal spread [1]. The aggressiveness of this cancer might be related to lymphotropism and the inverse polarity of tumor cell clusters [1]. With breast IMPCs, many studies have reported the occurrence of lymphatic and lymph nodal spread, while a 69-95% prevalence of axillary lymph node metastases was also reported [4,15-20]. Microscopic lymphatic vessel invasion is an independent adverse prognostic factor and is a marker of lymph node metastasis [4,15,19]. The frequency of lymphovascular invasion is reported to be approximately 55-76% [4,6, 20]. In our study, the frequency of lymph node metastasis was similar to that reported in the previous studies, which found the frequency to be 65.5% (19 of 29).

IMPC is characterized by higher rates of ER and PR expression [4,16,19,21]. Although ER positivity is generally known to be associated with better differentiation of tumors and an improved outcome, IMPCs seem to be an exception [4]. Zekioglu et al. [4] reported the percentages of ER and PR positivity to be 68% and 61%, respectively, for IMPCs. These results are surprisingly higher than those observed for IDCs. The reported prevalence of c-erbB-2 and p53 proteins (54% and 48%, respectively) was slightly higher than those of common breast cancers [4]. Walsh and Bleiweiss [19] reported high percentages of ER and PR positivity (90% and 70%, respectively) and nearly double the expected percentage of c-erbB-2 positivity (60%). In our study, the expressions of ER (27 of 29; 93.1%) and c-erbB-2 (15 of 29; 51.7%) were high, and similar to the results of the aforementioned studies [4,19]. Although many studies report higher incidences of ER and PR positivity for IMPCs, some studies have reported a lower frequency of ER expression for IMPCs [15]. These studies claim that some prognostic markers, such as ER, PR, p53, and c-erbB-2, cannot discriminate IMPCs from other breast cancers [4,15]. Hormone receptor status is one of the important prognostic factors for breast cancer and it has an important role in determining postoperative adjuvant therapy [22]. Positivities of p53 and c-erbB-2 are associated with the development of breast cancer and they are also associated with survival and prognosis [22-26]. Even though immunohistochemical profiles of IMPCs are not used to discriminate these tumors from other breast cancers, immunohistochemical studies can play an important role in treatment management and the indication of prognosis.

There are some limitations in our study. First, the study lacks a control group composed of patients who were diagnosed with IDC, not otherwise specified (IDC, NOS). A comparison of IMPC with IDC, NOS should precede an analysis of the character of IMPC. A second limitation of this study is that it is retrospective, so not all patients underwent imaging of their tumors with all four modalities.

In summary, imaging findings for IMPCs with mammography, US, and MRI are highly suggestive of malignancy, even though no features to distinguish IMPC from typical IDC were found. We identified the presence of frequent nodal metastases, high positivity of ER and c-erbB-2, and a high SUVmax value from PET-CT. These characteristics could be helpful in the treatment of and prognostic prediction for IMPCs.

CONFLICT OF INTEREST

The authors declare that they have no competing interests.

REFERENCES

1. Petersen JL. Breast carcinomas with an unexpected inside-out growth pattern: rotation of polarization associated with angioinvasion. Pathol Res Pract 1993;189:A780.
2. Adrada B, Arribas E, Gilcrease M, Yang WT. Invasive micropapillary carcinoma of the breast: mammographic, sonographic, and MRI features. AJR Am J Roentgenol 2009;193:W58-63.
3. Siriaunkgul S, Tavassoli FA. Invasive micropapillary carcinoma of the breast. Mod Pathol 1993;6:660-2.
4. Zekioglu O, Erhan Y, Ciris M, Bayramoglu H, Ozdemir N. Invasive micropapillary carcinoma of the breast: high incidence of lymph node metastasis with extranodal extension and its immunohistochemical profile compared with invasive ductal carcinoma. Histopathology 2004; 44:18-23.
5. Gunhan-Bilgen I, Zekioglu O, Ustün EE, Memis A, Erhan Y. Invasive micropapillary carcinoma of the breast: clinical, mammographic, and sonographic findings with histopathologic correlation. AJR Am J Roentgenol 2002;179:927-31.
6. Kim DS, Cho N, Ko ES, Kim DY, Yang SK, Kim SJ, et al. Imaging and the clinical-pathologic features of invasive micropapillary carcinoma of the breast. J Korean Radiol Soc 2007;56:497-503.
7. Yang WT, Chang J, Metreweli C. Patients with breast cancer: differences in color Doppler flow and gray-scale US features of benign and malignant axillary lymph nodes. Radiology 2000;215:568-73.

8. Tavassoli FA, Devilee P, International Agency for Research on Cancer, World Health Organization. Pathology and Genetics of Tumours of the Breast and Female Genital Organs. Lyon: IAPS Press; 2003. p.35-6.
9. Guo X, Chen L, Lang R, Fan Y, Zhang X, Fu L. Invasive micropapillary carcinoma of the breast: association of pathologic features with lymph node metastasis. Am J Clin Pathol 2006;126:740-6.
10. Wong SI, Cheung H, Tse GM. Fine needle aspiration cytology of invasive micropapillary carcinoma of the breast. A case report. Acta Cytol 2000;44:1085-9.
11. Gil-Rendo A, Martínez-Regueira F, Zornoza G, García-Velloso MJ, Beorlegui C, Rodriguez-Spiteri N. Association between [18F]fluorodeoxyglucose uptake and prognostic parameters in breast cancer. Br J Surg 2009;96:166-70.
12. Ueda S, Tsuda H, Asakawa H, Shigekawa T, Fukatsu K, Kondo N, et al. Clinicopathological and prognostic relevance of uptake level using 18F-fluorodeoxyglucose positron emission tomography/computed tomography fusion imaging (18F-FDG PET/CT) in primary breast cancer. Jpn J Clin Oncol 2008;38:250-8.
13. Cermik TF, Mavi A, Basu S, Alavi A. Impact of FDG PET on the preoperative staging of newly diagnosed breast cancer. Eur J Nucl Med Mol Imaging 2008;35:475-83.
14. Choi WH, Kim SH, Yoo LR, Park YH, Lee SY, Sohn HS, et al. Pre-operative FDG PET/CT findings related to early tumor recurrence in breast cancer patients. The Society of Nuclear Medicine 54th Annual Meeting. 2007. Abstract #47.
15. Kim MJ, Gong G, Joo HJ, Ahn SH, Ro JY. Immunohistochemical and clinicopathologic characteristics of invasive ductal carcinoma of breast with micropapillary carcinoma component. Arch Pathol Lab Med 2005; 129:1277-82.
16. Luna-Moré S, de los Santos F, Bretón JJ, Cañadas MA. Estrogen and progesterone receptors, c-erbB-2, p53, and Bcl-2 in thirty-three invasive micropapillary breast carcinomas. Pathol Res Pract 1996;192:27-32.
17. Nassar H, Wallis T, Andea A, Dey J, Adsay V, Visscher D. Clinicopathologic analysis of invasive micropapillary differentiation in breast carcinoma. Mod Pathol 2001;14:836-41.
18. Paterakos M, Watkin WG, Edgerton SM, Moore DH 2nd, Thor AD. Invasive micropapillary carcinoma of the breast: a prognostic study. Hum Pathol 1999;30:1459-63.
19. Walsh MM, Bleiweiss IJ. Invasive micropapillary carcinoma of the breast: eighty cases of an underrecognized entity. Hum Pathol 2001;32: 583-9.
20. Yu JH, Kim SW, Han WS, Kim SW, Park IA, Youn YK, et al. Micropapillary carcinoma of breast. J Korean Breast Cancer Soc 2004;7:132-5.
21. Tresserra F, Grases PJ, Fábregas R, Férnandez-Cid A, Dexeus S. Invasive micropapillary carcinoma. Distinct features of a poorly recognized variant of breast carcinoma. Eur J Gynaecol Oncol 1999;20:205-8.
22. Kim JK, Song YJ, Cho SI, Ryu DH, Yun HY, Sung RH. Clinicopathologic significance of p53 and c-erbB-2 protein expression in breast carcinoma. J Korean Breast Cancer Soc 2002;5:59-64.
23. Barbati A, Cosmi EV, Sidoni A, Collini P, Porpora MG, Ferri I, et al. Value of c-erbB-2 and p53 oncoprotein co-overexpression in human breast cancer. Anticancer Res 1997;17:401-5.
24. Bebenek M, Bar JK, Harlozinska A, Sedlaczek P. Prospective studies of p53 and c-erbB-2 expression in relation to clinicopathological parameters of human ductal breast cancer in the second stage of clinical advancement. Anticancer Res 1998;18(1B):619-23.
25. Bertheau P, Steinberg SM, Merino MJ. C-erbB-2, p53, and nm23 gene product expression in breast cancer in young women: immunohistochemical analysis and clinicopathologic correlation. Hum Pathol 1998; 29:323-9.
26. Ross JS, Fletcher JA. The HER-2/neu oncogene: prognostic factor, predictive factor and target for therapy. Semin Cancer Biol 1999;9:125-38.

http://dx.doi.org/10.4048/jbc.2012.15.1.57